A New Representation of fMRI Signal by a Set of Local Meshes for Brain Decoding

Itir Onal, *Student Member, IEEE*, Mete Ozay, *Member, IEEE*, Eda Mizrak, Ilke Oztekin, and Fatos T. Yarman Vural, *Senior Member, IEEE*

***Abstract*—How neurons influence each other's firing depends on the strength of synaptic connections among them. Motivated by the highly interconnected structure of the brain, in this study, we propose a computational model to estimate the relationships among voxels and employ them as features for cognitive state classification. We represent the sequence of functional Magnetic Resonance Imaging (fMRI) measurements recorded during a cognitive stimulus by a set of local meshes. Then, we represent the corresponding cognitive state by the edge weights of these meshes each of which is estimated assuming a regularized linear relationship among voxel time series in a predefined locality. The estimated mesh edge weights provide a better representation of information in the brain for cognitive state or task classification. We examine the representative power of our mesh edge weights on visual recognition and emotional memory retrieval experiments by training a support vector machine classifier. Also, we use mesh edge weights as feature vectors of inter-subject classification on Human Connectome Project task fMRI dataset, and test their performance. We observe that mesh edge weights perform better than the popular fMRI features, such as, raw voxel intensity values, pairwise correlations, features extracted using PCA and ICA, for classifying the cognitive states.**

***Index Terms*—Brain decoding, classification, functional magnetic resonance imaging (fMRI), voxel connectivity.**

I. Introduction

Functional Magnetic Resonance Imaging (fMRI) is used as the primary modality to capture neural activations in the brain due to its high spatial resolution and reasonable temporal resolution [1]. It measures the Blood Oxygenation Level Dependent (BOLD) responses obtained from voxels, the smallest units of brain volumes from which fMRI measurements can be recorded, for each repetition time (TR).

The techniques employed to learn the brain activity patterns from the BOLD signals became popular in the last few decades and these techniques are recently called as Multi Voxel Pattern Analysis (MVPA). Following the pioneering study of Haxby *et al.* [2], machine learning techniques have been used for diagnosing disorders [3], [4], hypothesis validation [5] and classifying cognitive states which is a method for predicting cognitive states, called brain decoding.

In traditional MVPA approaches, cognitive states are usually represented by concatenating the selected voxel intensity values to construct a vector in a feature space. The time series recorded at each voxel can be represented by various methods, such as computing maximal or mean values. Also, dimension of the feature space can be reduced by Principal Component Analysis (PCA) and Independent Component Analysis (ICA). Then, a classifier, such as, Support Vector Machine (SVM), k-Nearest Neighbor (k-NN) or Naive Bayes, is trained by the feature vectors.

State-of-the-art models adopt machine learning algorithms to design models for brain decoding problems [6]. For example, Graphnet [7] and TV-l1 [8], [9] methods suggest a spatial regularization technique for regression and classification problems of brain imaging.

In addition to designing models, there exists a number of techniques to extract meaningful information from fMRI signals. A popular method for extracting a spatial feature from fMRI data is to average the BOLD response at each voxel to represent a stimulus [10]–[12]. A recent work, suggested by Ng *et al.* [13], [14], considers each brain volume as a sample. On the other hand, Mitchell *et al.* [15] and Ng *et al.* [16] concatenate the BOLD responses within the same trial to extract features that include spatio-temporal information.

In order to extract the temporal information from the fMRI data, various studies [17]–[21] compute the pairwise correlations between the responses of voxels or brain regions. Among these studies, Pantazatos *et al.* [17] model temporal relationships by using pairwise correlations between brain regions as features for brain decoding. Moreover, Richiardi *et al.* [18] model a functional connectivity graph using the pairwise correlations between brain regions, and they decode the brain states using graph matching algorithms. The edge weights of their brain graph are generally selected using the correlation between pairs of selected regions, and vertices or edge weights of the brain graphs are used as features for cognitive state classification [22]. In addition to the coarse-level functional connectivity, Firat *et al.* [19] suggested pairwise correlations of voxels as features while Baldassano *et al.* [20] extract the functional connectivity

Manuscript received February 21, 2017; accepted March 3, 2017. Date of publication March 8, 2017; date of current version November 3, 2017. This work was supported in part by TUBITAK under Grant 114E045 and in part by CREST, JST. The work of I. Onal was supported by TUBITAK. The associate editor coordinating the review of this manuscript and approving it for publication was Prof. P. M. Djuric.

I. Onal and F. T. Y. Vural are with the Department of Computer Engineering, Middle East Technical University, 06800 Ankara, Turkey (e-mail: itir@ceng.metu.edu.tr; vural@ceng.metu.edu.tr).

M. Ozay is with the Graduate School of Information Sciences, Tohoku University, Sendai 980-8577, Japan (e-mail: ozay.mete.b4@tohoku.ac.jp).

E. Mizrak and I. Oztekin are with the Department of Psychology, Koc University, 34450 Istanbul, Turkey (e-mail: emizrak@ku.edu.tr; ioztekin@ku.edu.tr).

Color versions of one or more of the figures in this paper are available online at http://ieeexplore.ieee.org.

Digital Object Identifier 10.1109/TSIPN.2017.2679491

structures by modeling pairwise connectivity among voxels. Also, a minimum spanning tree of a graph structure defined by a functional connectivity matrix between all voxel pairs is employed to represent a stimulus for brain decoding [21]. Note that, the aforementioned temporal methods are designed to model only the pairwise relationships between voxels and employ these relationships as features for brain decoding. Although these methods represent the spatio-temporal information to a certain degree, none of them represents the spatial relationships among the brain volumes, recorded along the time course of a cognitive stimulus. In other words, spatial models mostly lack the temporal information while the temporal ones lose the spatial relationships among the voxel BOLD responses.

The major motivation of this study follows the observation that the strength of synaptic connections fundamentally determines how neurons influence each other's firing [23]. Although a neuron makes weak connections with a large number of other neurons, it obtains its local excitation from strong inputs provided by few neurons that give similar responses to the same stimuli. Therefore, there exist spatial and temporal relationships among neurons residing within a locality, and the strength of these relationships determines the strength of neural response. It is observed that, at a coarser level, voxel BOLD responses are functionally and spatially correlated in pre-defined local structures, i.e. functional and spatial neighborhoods. As an example, Bazargani *et al.* [24] state that neighboring voxels belonging to a homogeneous ROI have Hemodynamic Response Function (HRF) with the same shape, possibly with slightly varying amplitude. In other words, spatially close voxels tend to give similar BOLD responses to the same stimuli. Moreover, Kriegeskorte *et al.* [25] report that a univariate model of activations fails to benefit from local spatial combination of signals, and performs worse than Searchlight methods for detection of informative regions. They observe that spatially remote voxels may also exhibit functionally similar time series.

Furthermore, Ozay *et al.* [26] observe that the voxel time series do not differ significantly to discriminate the different cognitive states, but there exist slight variations among the voxel intensity values of voxels located in a spatial neighborhood. They propose a set of Local Meshes (LMM) to model the relationship among the spatially close voxels. They show that the LMM features perform better than the voxel intensity values for the classification of cognitive states. However, in [26], only the brain volume which is obtained 6 s after the stimulus presentation is used for the construction of a model while the remaining ones are discarded under the canonical HRF assumption.

Finally, Firat *et al.* [27] propose a Functional Mesh Model (FMM) which is used to construct a set of local meshes by selecting the nearest neighbors of voxels defined within a functional neighborhood. Their experimental results show that their features are more discriminative than the ones obtained within a spatial neighborhood. Yet, they also estimate the mesh weights using only a single intensity value for each voxel.

In none of the above mentioned models, the time series recorded at all the voxels are fully employed to represent the spatial relationships among the voxels of the fMRI data. The available approaches either use the active voxels or the most crucial time instances or both. Although these approaches smooth the noise in voxel time series, and represent the huge amount of data in a more compact way, it may result in losing important information embedded in time series of brain volumes, recorded under a stimulus.

The massively interconnected and dynamic nature of human brain cannot be represented by considering only a collection of selected voxels and/or time instances which are obtained from fMRI data. In addition, the above mentioned studies indicate that the relationship among the voxels is more informative than the information provided by the individual voxels. Therefore, it is desirable to develop a model which represents the relationship among the voxel time series of fMRI signal, recorded during a stimulus.

In this study, we employ the voxel time series measured during a cognitive task to create a local mesh around each voxel which models the relationship among the BOLD responses. The concept of locality is defined over a neighborhood system. We introduce two types of neighborhoods, namely, spatial and functional neighborhoods. We construct a local mesh around each voxel by using either a spatial [28] or functional neighborhood system to generate a set of spatially or functionally local meshes. We form a local mesh around each voxel by connecting the voxel to its p-nearest neighbors under a star topology. In each mesh, we represent the BOLD response of a voxel by a regularized linear combination of BOLD responses of its spatially or functionally nearest neighbors. We estimate the mesh edge weights by solving a ridge regression equation. The mesh edge weights estimated for each voxel enable us to represent the fMRI brain volumes recorded during a stimulus by a graph which consists of an ensemble of local meshes.

The proposed local mesh models are different from the connectivity models defined over pairwise similarities between voxels and/or regions in the sense that the connectivity is defined over a local neighborhood of voxels. We employ the estimated weights of mesh edges as features to train and test the state-of-the-art Support Vector Machines (SVM) for decoding a set of cognitive processes measured by fMRI signals.

We test our approach in two event-related design experiments, namely, visual recognition and emotional memory retrieval experiments. Moreover, we perform cognitive task classification, where each task contains a few hundreds of measurements on Human Connectome Project (HCP) task fMRI dataset. We observe that the classifiers which employ the proposed local mesh ensembles outperform the state of the art MVPA features.

In Fig. 1, the steps of the proposed method are summarized. First, we preprocess the fMRI measurements and obtain voxel intensity values. Then, we select voxels or anatomic regions to eliminate the redundancies and to reduce the noise in our dataset. After that, we define spatial and functional neighborhood systems, and construct meshes, accordingly. Finally, we estimate edge weights of meshes, and input them to a classifier to train and test the cognitive states.

II. Neuroimaging Data Collection

In this study, three sets of fMRI data is tested to observe the power of the suggested mesh representation for brain decoding problems. The first two datasets, namely, visual object

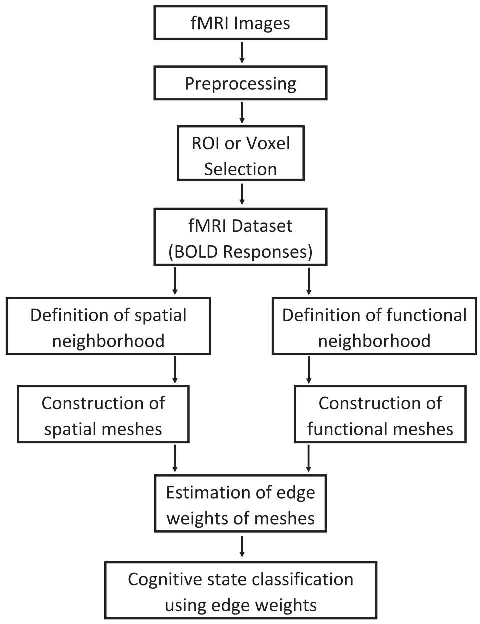

Fig. 1. The flowchart of the proposed approach for obtaining local meshes and classification of cognitive states.

recognition and emotional memory retrieval experiments are designed and recorded by our team. The third dataset is taken from Human Connectome Project (HCP).

A. Visual Object Recognition Experiment

In this experiment, fMRI measurements were recorded while participants performed a one-back repetition detection task. The stimuli consist of gray-scale images belonging to two categories, namely, birds and flowers. Each trial lasts for 12 s containing stimulus presentation for 4 s, and a following rest period of 8 s. Scanning was performed on a Siemens 3T Magnetom TRIO MRI system. Functional images were acquired using a gradient EPI sequence (TR $=$ 2000 msec, TE $=$ 30 msec, flip angle $=$ 90, 34 interleaved axial slices, voxel size $=$ 3 mm $\times$ 3 mm $\times$ 3 mm with 0.3 mm interslice gap). Since our TR $=$ 2 seconds, we obtain 6 measurements (scan volumes) for each trial.

This experiment consisted of 6 runs (sessions), and each run contains 36 trials. Therefore, we obtained a total of 216 trials (each having 6 measurements) for a single participant. A total of 1512 images were collected for a single participant. We collected data from 5 participants.

B. Emotional Memory Retrieval Experiment

In this experiment, the stimuli consist of two neutral (Kitchen utensils and Furniture) and two emotional (Fear and Disgust) categories of images. Each trial started with a 12 seconds fixation period followed by a 6 seconds encoding period. In the encoding period, participants were presented with 5 images from the same category, each image lasting 1200 ms on the screen. Following the fifth image, a 12 seconds delay period was presented in which participants solved three math problems consisting of addition or subtraction of two randomly selected two-digit numbers. Following the third math problem, a 2 seconds retrieval period started in which participants were presented with a test image from the same category, and indicated whether the image was a member of the current study list or not. For a similar experimental setting, please refer to [29].

This experiment consisted of 6 19-min runs and each run contains 35 trials. A total of 210 trials and 3456 images were obtained for a single participant. Scanning was performed on a Siemens 3T Magnetom TRIO MRI system. Functional images were acquired using a gradient EPI sequence (TR $=$ 2000 msec, TE $=$ 30 msec, flip angle $=$ 90, 34 interleaved axial slices, voxel size $=$ 3 mm $\times$ 3 mm $\times$ 3 mm with 0.3 mm interslice gap). We collected data from 13 participants. We employ 6 measurements (6 seconds of encoding and 6 seconds of following rest) of each trial for classification. Notice that, we only employ the data obtained during the encoding phase.

TABLE I
NUMBER OF SCANS PER SESSION AND ITS DURATION FOR EACH TASK (MIN:SEC) FOR HCP DATA

	Emotion	Gambling	Language	Motor	Relational	Social	WM
Scans	176	253	316	284	232	274	405
Duration	2:16	3:12	3:57	3:34	2:56	3:27	5:01

C. Human Connectome Project (HCP) task fMRI Data

We use task fMRI data of Human Connectome Project (HCP) collected from 808 participants. During the experiments the participants performed seven tasks namely Emotion Processing, Gambling, Language, Motor, Relational Processing, Social Cognition, Working Memory (WM) [30]. Note that the number of scans and their duration vary for each task yet we obtain equal duration for all participants (see Table I). Although, there are total of 900 subjects in HCP task fMRI data release, 808 of them performed all of the 7 tasks. Therefore, we use the data obtained from 808 participants, and we discard the data obtained from the remaining participants.

In this experiment, we define *supervoxels* such that we average BOLD responses of voxels residing in the same anatomical region, and denote each *supervoxel* with that average time series. We use $R = 90$ anatomical regions of 116 AAL [31], after removing anatomical regions of Cerebellum and Vermis. Therefore, in our experiments, we have 90 *supervoxels*. Since our aim is to classify cognitive experiments rather than cognitive states within an experiment, we work in coarser granularity. Moreover, using this dataset, we perform inter-subject classification to see how well our framework performs for multi-subject classification.

III. PREPROCESSING AND ANALYSIS OF NEUROIMAGING DATA

SPM8 is used for preprocessing and analysis of fMRI datasets.[1] Preprocessing of images consists of (a) correction of slice acquisition timing across slices, (b) realigning the images

[1] http://www.fil.ion.ucl.ac.uk/spm/

to the first volume in each fMRI run to correct for head movement, (c) normalization of functional and anatomical images to a standard template EPI provided by SPM2, and (d) smoothing images with a 6-mm full-width half-maximum isotropic Gaussian kernel. Finally, we extract 116 Automated Anatomical Labeling (AAL) regions [31] using Marsbar [32]. For the visual object recognition and emotional memory retrieval datasets, General Linear Model is implemented to find the distribution of active voxels across the anatomic regions. The active voxels in object recognition dataset are mostly located in occipital lobe, which is selected as the region of interest (ROI) for this experiment. On the other hand, the active voxels in the emotional memory retrieval dataset are scattered all over the brain regions. The most discriminative voxels are, then, selected by t-test among all the voxels of this dataset. We first split samples into two groups according to their class labels. Then, we compute p-values for each voxel that reflects how the two groups are well-separated by each voxel. We select 800 voxels since almost 800 of them have $p < 0.005$. We perform voxel selection repetitively for each training split of nested cross validation. For HCP dataset, rather than selecting the active voxels, we employ all of the 90 anatomical regions in the form of *supervoxels*, each of which is represented by the average region time series. This is a widely-accepted approach for the datasets, such as HCP, which consist of task experiments of long duration.

IV. Mesh Representation of fMRI Signal With Respect to Functional and Spatial Neighborhoods

The local mesh representation of fMRI signal, proposed in this study, is constructed using a collection of voxels located within a neighborhood of each voxel. For this purpose, first we make a formal definition of locality. This task is achieved by defining spatial and functional neighborhood systems. Then, we define local meshes and based on the neighborhood we obtain two types of meshes namely, spatially and functionally local meshes. In the following sub-sections, we provide the formal definition of neighborhood systems, construction of local meshes and the estimation of mesh edge weights.

A. Neighborhood Systems

One of the most important tasks of this study is to construct a linear relationship among the BOLD responses of voxels by employing ”locality” properties of the voxels. In order to achieve this goal, we define two types of neighborhood systems, namely, spatial and functional neighborhoods. In the case of spatial neighborhood, we compare 3-dimensional coordinates of voxels and in the functional case, we define similarity measures to compare voxel time series.

Definition 1 (Spatial Neighborhood): For each voxel v, we define the spatial neighborhood centered in v with a radius π by $\eta(v, \pi) = \{u \in V | d(v, u) < \pi\}$ where V denotes the set of voxels and $d(v, u)$ denotes the Euclidean distance between the spatial coordinates of v and u in 3-dimensional space.

Definition 2 (Functional Neighborhood): Let $X_v(t)$ denote the time series of BOLD responses obtained from voxel v which is recorded as the response of a series of stimulus during the entire experiment. In order to find the functionally nearest neighbor of a voxel v, we compute similarity between voxel time series $X_v(t)$ and $X_u(t)$ for all the voxel pairs $v, u \in V$. Then, we select p-functionally nearest neighbors of a voxel as the voxels having p of the highest similarity with v. In this study, we employ Pearson correlation, partial correlation and Granger causality as functional similarity measures.

Fig. 2 shows examples of meshes formed within spatial and functional neighborhood. Note that functionally p-nearest neighbors of a voxel may or may not be the same as the spatially p-nearest neighbors. Practical evidence indicates that most of the spatially close voxels are also functionally similar. However, some of the voxel pairs are spatially far apart, yet they are functionally close to each other (see Fig. 2(b)).

B. Construction of Local Meshes

Based upon the neighborhood systems introduced in the previous section, the concept of locality is represented by a set of meshes defined over a sequence of brain volumes. For this purpose, two types of meshes, namely, spatially and functionally local meshes, are established.

Both types of meshes are constructed around each voxel of the brain volume using a predefined neighborhood system. Once we select the neighborhood system, we form a local mesh around each voxel by connecting the voxel to its neighboring voxels in a star topology. The voxel located at the center of a mesh is called the *seed voxel*. Since we form the meshes around all of the voxels in the brain volume, the meshes defined over a neighborhood system may overlap. A seed voxel in a mesh may become a neighboring voxel of a seed voxel in a different mesh.

The formal definition of the local meshes are given below:

Definition 3 (Local Meshes): For each voxel v in the brain volume, a local mesh is defined as $\mathcal{M}_v = (\mathcal{V}, \mathcal{E})$ where $\mathcal{V}_v = \{v \cup \eta_p[v]\}$ represents a set of the voxels of the mesh, and

$$\mathcal{E}_v = \{e_{vu} : \forall u \in \eta_p[v]\}$$

is a set of edges formed between the seed voxel v of the mesh and its p-nearest neighbors (see Fig. 3).

When the spatial neighbors are used to form meshes, we call them Spatially Local Meshes (SLM) (see Fig. 3). On the other hand, when the nearest neighbors are selected based on the similarity of voxel time series, we call the meshes Functionally Local Meshes (FLM) (see Fig. 4).

For FLM, the same star topology is defined for all meshes with a fixed mesh size p. On the other hand, for SLM, different voxels may have different number of neighbors due to the definition of spatial neighborhood and topology of 3-dimensional locations of voxels. In both cases, the voxels and the edges formed between them in a mesh do not change in time. However, the voxel intensity values measured for each entry of the time-series representing the BOLD response, change in time. Since we estimate a set of edge weights for each cognitive stimulus, they remain the same for the duration of a stimulus and only change across the stimuli.

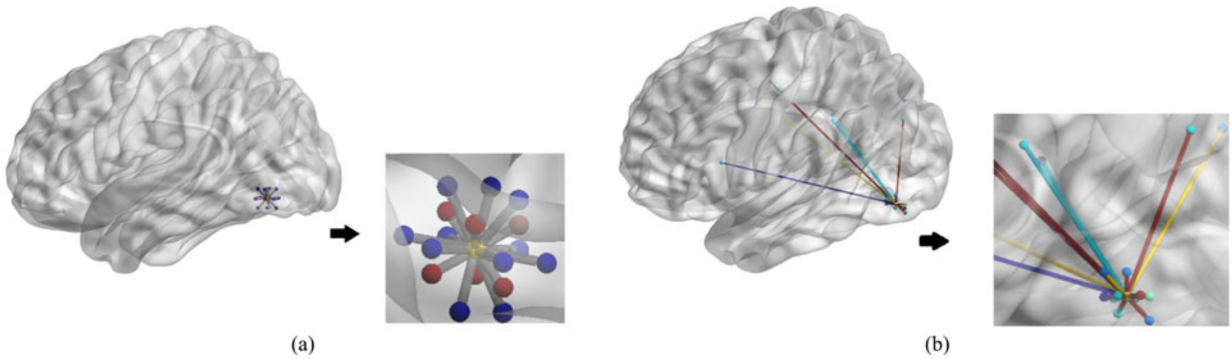

Fig. 2. A local mesh formed by (a) spatial neighbors and (b) functional neighbors of a seed voxel. In both figures, the voxel denoted with yellow color at the center is the seed voxel. In (a), red voxels denote the spatially nearest neighbors of the yellow voxel within a radius of 1 unit and blue voxels have $\sqrt{2}$ unit distance to yellow voxel. In (b), we have a mesh formed with functional neighbors around the seed voxel denoted with yellow color. (a) Spatially local meshes. (b) Functionally local meshes.

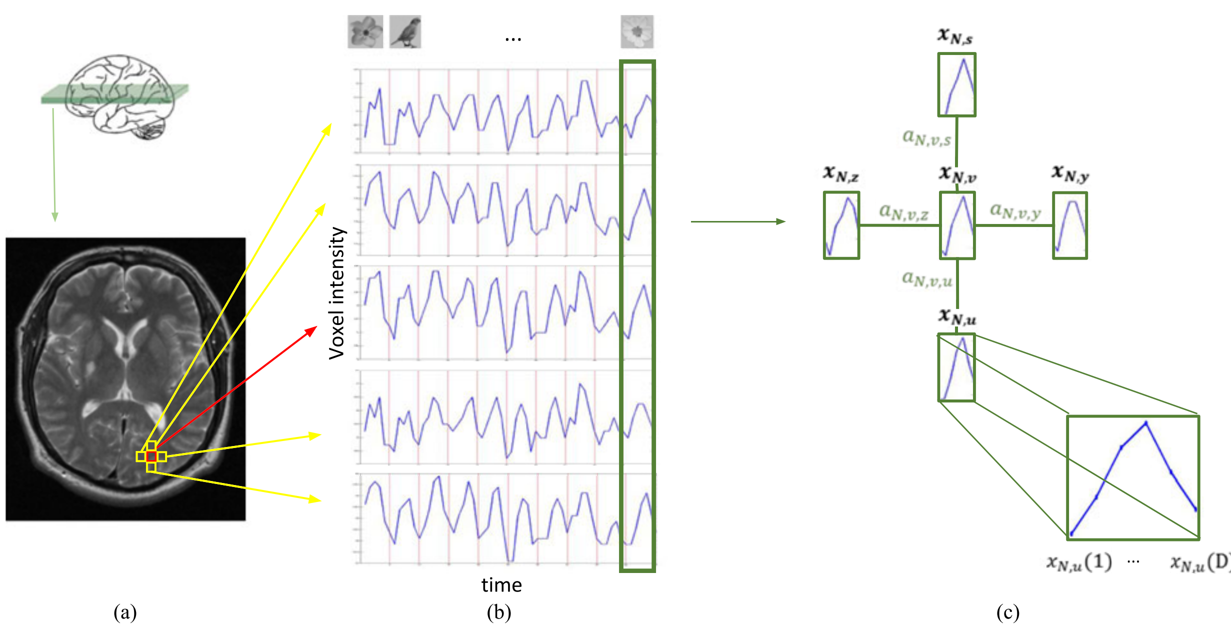

Fig. 3. Design of a spatially local mesh for modeling the relationship among the BOLD responses of voxels. (a) For simplicity, a seed voxel is depicted in an axial slice at the center of a mesh (red) with its four spatially nearest neighbors (yellow). Neighboring voxels are selected within a 3D brain volume. (b) fMRI time series are recorded at each voxel, for each stimulus for bird and flower classes. (c) A local mesh is computed using the responses obtained from a seed voxel $\boldsymbol{x}_{\boldsymbol{N},\boldsymbol{v}}$ and its four nearest neighbors for the last sample N. We also visualize voxel intensity values of a sample response $\boldsymbol{x}_{\boldsymbol{N},\boldsymbol{u}}$ obtained from voxel u.

Once we define a mesh around each voxel, we address the problem of estimating the edge weights. The proposed edge estimation method is explained next.

C. Estimation of Edge Weights of Meshes

Suppose that we record the BOLD response at a voxel v given to a stimulus within a window w in order to measure the brain activation for a predefined cognitive state with label c. We denote the intensity values of the BOLD response measured at a voxel v within window w by the vector $\boldsymbol{x}_{\boldsymbol{w},\boldsymbol{v}} = [x_{w,v}(t)]_{t=1}^{D}$. For each stimulus, we record D measurements.

We form meshes around voxels for each window. For a window, we denote the estimated weight of an edge between seed voxel of a mesh v and a neighboring voxel u by $a_{w,v,u}$. We estimate the edge weights for both spatially and functionally local meshes in the same way. When we concatenate the BOLD responses of all stimuli, we obtain a vector $X_v(t) = [\boldsymbol{x}_{\boldsymbol{w},\boldsymbol{v}}]_{\forall w}$ of BOLD responses measured from a voxel v for all windows of training samples. Recall that, we employ $X_v(t)$ to select functional neighbors using correlations.

We represent a mesh formed among the BOLD response of a seed voxel v of the mesh, and the BOLD responses of its p-nearest neighbors for a window w as:

$$\hat{\boldsymbol{x}}_{\boldsymbol{w},\boldsymbol{v}} = \sum_{u \in \eta_p[v]} a_{w,v,u}\, \boldsymbol{x}_{\boldsymbol{w},\boldsymbol{u}}, \tag{1}$$

where $\hat{\boldsymbol{x}}_{\boldsymbol{w},\boldsymbol{v}}$ denotes the estimated BOLD response vector of voxel v for window w. We estimate the edge weights of a mesh

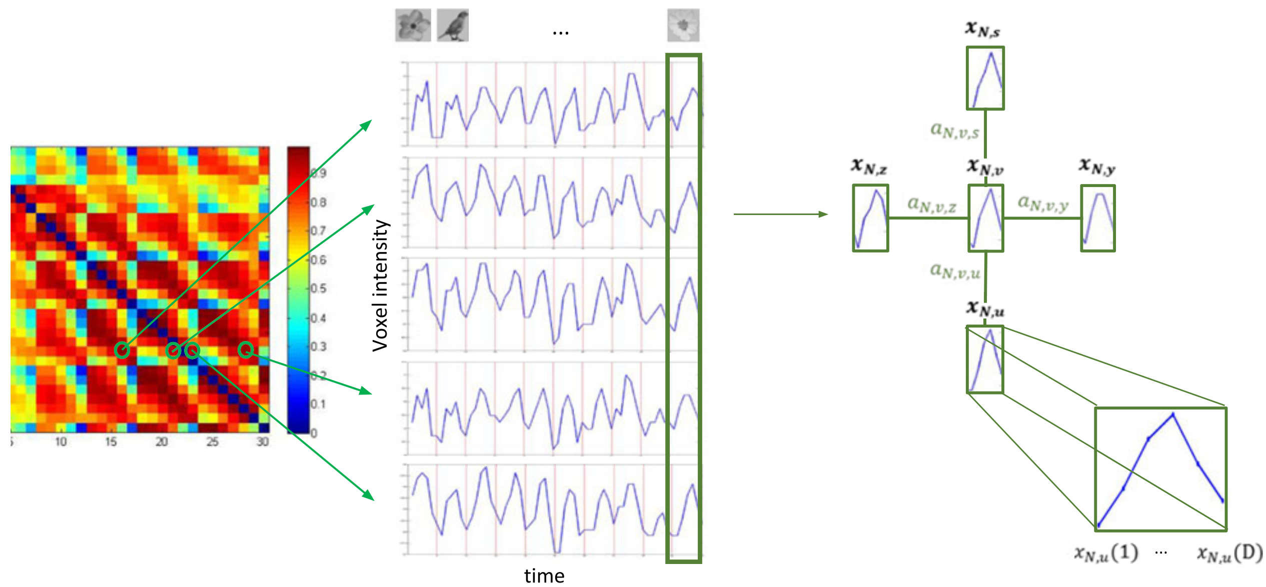

Fig. 4. Design of a functionally local mesh using the voxel time series. (a) A sample functional connectivity matrix formed using Pearson correlation. p-functionally nearest neighbors of a voxel are denoted as the ones with the dark-to-light red colors. (b) fMRI measurements are recorded for each stimulus for bird and flower classes. (c) We depict a functional mesh formed around a seed voxel, in star topology. The edge weights are computed by using the response obtained from a seed voxel $\boldsymbol{x_{N,v}}$ and the responses of its four functionally nearest neighbors, $\boldsymbol{x_{N,s}}$, $\boldsymbol{x_{N,u}}$, $\boldsymbol{x_{N,y}}$, $\boldsymbol{x_{N,z}}$, for the last sample N.

formed around a voxel v for a window w by minimizing the regularized linear model error as follows:

$$\min_{a_{w,v,u}} \left(||\hat{\boldsymbol{x}}_{\boldsymbol{w},\boldsymbol{v}} - \boldsymbol{x}_{\boldsymbol{w},\boldsymbol{v}}||^2 + \lambda\ ||a_{w,v,u}||^2\right) \tag{2}$$

where $\lambda \in \mathbb{R}$ denotes regularization parameter. Notice that η_p corresponds to η_p^{spat} if meshes are formed considering spatial neighborhood, and corresponds to η_p^{func} if the meshes are formed considering functional neighborhood. We compute an edge vector $\boldsymbol{a}_{\boldsymbol{w},\boldsymbol{v}} = [a_{w,v,1}, a_{w,v,2}, \ldots, a_{w,v,p}]$ using ridge regression as

$$\boldsymbol{a}_{\boldsymbol{w},\boldsymbol{v}} = (Q_{w,v}^T Q_{w,v} + \lambda I)^{-1} Q_{w,v}^T \boldsymbol{x}_{\boldsymbol{w},\boldsymbol{v}}, \tag{3}$$

where $Q_{w,v}$ is a $D \times p$ matrix consisting of BOLD responses obtained from p-nearest neighbors of a seed voxel v for window w such that

$$Q_{w,v} = [\boldsymbol{x}_{\boldsymbol{w},\boldsymbol{u}}],\ \forall u \in \eta_p[v]. \tag{4}$$

V. Classification of Cognitive States For Brain Decoding

The representation power of the proposed mesh ensemble is analyzed in the fMRI recordings during a number of brain decoding tasks. The major question is then how well a cognitive state can be represented by the ensemble of meshes? The answer to this question can be partly observed from the performance of the classifier trained with mesh edge weights.

Recall that for each cognitive stimulus or task, we record a sequence of brain volumes obtained for a window. We estimate mesh edge weights for each window w, where w covers the BOLD responses obtained for each stimulus for visual recognition and emotional memory retrieval experiments. For HCP dataset, window w covers the duration D of a cognitive task, where durations can be found in Table I. Each stimulus or task is associated with a label c. Finally, each sample in the dataset is represented by a vector with the entries of the estimated mesh edge weights in the input space of a classifier.

Formally speaking, for each window w with label c, the edge weights $\boldsymbol{a}_{\boldsymbol{w},\boldsymbol{v}} \in \mathbb{R}^{1\times p}$ are used to construct a feature vector $F_w = [\boldsymbol{a}_{\boldsymbol{w},\boldsymbol{1}}, \boldsymbol{a}_{\boldsymbol{w},\boldsymbol{2}}, \ldots, \boldsymbol{a}_{\boldsymbol{w},|\boldsymbol{V}|}]$ by concatenating all edge weight vectors, where $|V|$ denotes the number of voxels. We employ F_w features to train and test classifiers.

VI. Brain Decoding Experiments Performed on the fMRI Datasets

In order to observe the validity of the proposed mesh representation, we perform two groups of experiments. In the first group, we train and test a Support Vector Machine (SVM) classifier by using the labeled fMRI data recorded using the experimental setups explained in Section II. In this group of experiments, we examine the power of the mesh edge weights for representing the brain states. In the second group of experiments, we analyze the validity of the local meshes by exploring the similarities among the voxel time series in each mesh, and the distribution of the error of the proposed regularized linear regression model.

A. Comparison of Mesh Weights With State-of-the-art fMRI Features

We compare the proposed spatial and functional mesh weights with the state-of-the-art features, by measuring the performance of the classifiers trained by these features. We train an SVM classifier with linear kernel, and classify an unknown stimulus.

We perform seven sets of classification experiments on three different groups of fMRI datasets:

1) In the first and second set of experiments, we represent a cognitive stimulus using the edge weights of meshes. The classification performances are measured when the edge weights obtained from the spatially **(SLM)** and functionally local meshes **(FLM)** are fed as the input of an SVM classifier.
2) In the third and fourth set of experiments, we tested the classification performances of SVM by employing features obtained using Local Mesh Model (**LMM**) and Functional Mesh Model (**FMM**). Recall that both **LMM** and **FMM** employ only a single measurement from the BOLD response for each voxel omitting the rest of the signals measured during a stimulus.
3) In the fifth group of experiments, we test the performance of SVM classifiers which employ features that are computed using pairwise Pearson correlation (**FC**). First, we compute the pairwise correlations between the voxel BOLD responses given by seed voxels and each of their p-nearest neighbors for each stimulus. In other words, first meshes are constructed around seed voxels, and then pairwise correlations are computed between voxel pairs within meshes instead of estimating the edge weights within a neighborhood. Then, we form our feature vector by concatenating the correlation values in all meshes. Note that, we obtain feature vectors whose sizes are equal to that of **SLM** and **FLM** by concatenating only the distances within meshes to make a fair comparison.
4) In the sixth set of experiments, we analyze the performance of SVM classifiers where raw voxel intensity values are used as features to train and test classifiers. For **RAW-mid**, we only used the third instance $x_{w,v}(3)$ in the middle of a BOLD response $\boldsymbol{x_{w,v}}$ following our assumption that if a voxel becomes active, then its HRF reaches to its peak value after 5–6 seconds (around $t = 3$). On the other hand, **RAW-mean** depicts the case where we employed the average of D measurements of $\boldsymbol{x_{w,v}}$. We also concatenate each of the D measurements of BOLD response $x_{w,v}(t)_{t=1}^{D}$ to obtain results for **RAW-all**. The dimension of a feature vector constructed for **RAW-mid** and **RAW-mean** equals to 1254 for visual object recognition experiment, 800 for emotional memory retrieval experiment and 90 for HCP task fMRI data. Moreover, since we concatenate all measurements for **RAW-all**, the size of the feature vectors used for **RAW-all** equals to D times the size of features vectors for **RAW-mean** and **RAW-mid**. Since each task of HCP data has different durations and we do not perform event-related task classification, we cannot employ **RAW-mid** and **RAW-all** experiments on HCP data.
5) In the seventh set of experiments, we extract features using Principal Component Analysis **(PCA)** and spatial Independent Component Analysis **(ICA)**. We map the fMRI data onto the first 100 components that retain 99% of the variance. Following **PCA**, we applied spatial **ICA** to our raw data using FastIca [33].

B. *Classification Results for Brain Decoding*

We perform intra-subject classification using SVM classifiers with visual object recognition and emotional memory retrieval experiments and inter-subject classification using HCP task fMRI dataset.

In visual object recognition and emotional memory retrieval experiments, we perform nested cross validation across runs [34]. The outer loop runs for 6 folds, and within each fold of the outer loop, an inner loop runs for 5 folds for parameter tuning. For each fold of the outer loop, we employ measurements obtained from 5 runs for decoding, and 1 run for test. For each fold of the inner loop, we divide the decoding part into 4 runs of training set and 1 run of validation set. We use the validation set to optimize the cost parameter, C of SVM and the regularization parameter λ. Similarly, we also optimize the number of neighbors p used for computation of functional neighborhoods and radius of neighborhoods π used for computation of spatial neighborhoods. After we estimate the parameters in the inner loop, we train classifiers using decoding part with the estimated *optimal* parameters, and measure the test performance using the unseen test set. We searched for the optimal values of λ in $\{0, 0.125, 0.25, 0.5, 1, 2, 4, 8\}$, SVM cost parameter C in $\{0.001, 0.01, 0.1, 1, 10, 100, 1000\}$ and π in $\{1, \sqrt{2}, \sqrt{3}\}$. We optimize the number of neighbors p in $\mathcal{P} = \{2, 3, \ldots, 30\}$ for visual object recognition experiment, and p in $\mathcal{S} = \{5, 6, \ldots, 15\}$ for emotional memory retrieval experiment.

For HCP task fMRI experiments, we split our data into 8 chunks, where each chunk contains fMRI data collected from 101 participants. We perform nested cross validation in which the outer loop runs for 8 folds, and within each fold of the outer loop, an inner loop runs for 7 folds for parameter tuning. We search for the optimal values of λ in $\{0, 32, 64, 128, 256, 512\}$, C in $\{0.001, 0.01, 0.1, 1, 10, 100, 1000\}$ and p in $\mathcal{T} = \{5, 10, 15, 20, 25, 30\}$ on the validation set. Since the data scale in these datasets is at region level, we searched for the optimal λ and p values in a different range during these experiments. Note that, unlike voxels, *supervoxels* are not located on a full grid. Therefore, we select the number of spatial neighbors from the set $\mathcal{T} = \{5, 10, 15, 20, 25, 30\}$ for HCP dataset.

We analyze the effect of similarity measures in subsection VI-C. As will be explained in this subsection, Pearson correlation provides relatively better decoding performances compared to partial correlation and Granger causality. For this reason, we conduct the experiments on **FLM** by just measuring Pearson correlation to select nearest neighbors.

Visual Object Recognition Experiment: We give the average classification performances of 6-fold obtained for visual object recognition experiment in Table II. Results reflect that **FLM** and **SLM** features discriminate brain states much better than other features.

Emotional Memory Retrieval Experiment: We provide performances for 2-class and 4-class classification experiments. In 2-class experiments the classes correspond to the neutral and emotional tasks (see Table III). In 4-class experiments, we

TABLE II
CLASSIFICATION PERFORMANCE (%) OF SVM CLASSIFIER COMPUTED IN VISUAL OBJECT RECOGNITION EXPERIMENT

Participant	FLM	SLM	FMM mean	FMM mid	LMM mean	LMM mid	FC	RAW mean	RAW mid	RAW all	PCA	ICA
1	91.42	**93.14**	73.14	80	70.29	74.28	72	74.85	78.29	75.43	73.71	86.29
2	**83.81**	81.43	67.14	68.09	68.57	73.33	71.90	71.90	74.76	76.19	73.33	79.52
3	**92.86**	83.33	67.62	75.71	68.57	78.09	53.33	70	75.71	76.67	70.48	79.52
4	**89.05**	76.67	71.90	75.23	73.33	74.76	62.38	74.29	78.57	70.48	72.86	87.62
5	**78.09**	81.43	68.57	75.71	63.33	71.43	57.14	68.09	70.48	67.62	68.57	75.71
Avg.	**87.04**	83.20	69.67	74.95	68.82	74.38	63.35	75.56	74.68	73.27	71.79	81.73

TABLE III
CLASSIFICATION PERFORMANCE (%) OF SVM CLASSIFIER COMPUTED IN EMOTIONAL MEMORY RETRIEVAL EXPERIMENT (2-CLASS)

Participant	FLM	SLM	FMM mean	FMM mid	LMM mean	LMM mid	FC	RAW mean	RAW mid	RAW all	PCA	ICA
1	**97.62**	97.14	80.48	83.33	78.10	80.48	84.29	81.43	76.19	92.86	74.76	94.29
2	**92.86**	90.95	79.52	80.48	77.62	79.52	76.19	83.81	75.24	90.48	73.81	82.85
3	**73.33**	69.52	67.14	55.71	60.48	50.48	61.90	57.14	50.48	67.62	58.57	64.76
4	**87.62**	**87.62**	73.33	65.71	77.62	67.14	76.67	62.38	56.67	73.33	65.24	78.57
5	**92.38**	91.90	77.62	61.43	72.86	56.19	84.29	66.19	54.76	71.43	64.76	83.81
6	**98.10**	97.62	71.43	74.76	81.90	81.90	89.05	66.19	68.57	79.05	72.86	88.57
7	**92.86**	**92.86**	65.24	67.62	64.29	65.24	80.00	63.81	56.67	81.90	72.86	85.24
8	**90.00**	89.05	66.19	63.33	68.10	56.67	79.05	67.14	60.00	79.05	63.33	78.57
9	90.00	90.00	79.52	72.86	80.48	69.52	78.57	79.05	72.38	**94.76**	71.90	90.48
10	**93.81**	89.52	71.43	65.24	72.38	54.76	74.76	61.43	59.52	74.29	63.33	79.52
11	**95.24**	**95.24**	69.05	70.00	67.62	67.62	89.05	75.71	78.10	87.14	79.05	93.81
12	78.57	77.62	71.90	61.90	76.67	62.38	78.10	63.81	66.67	75.71	80.95	**98.10**
13	**96.67**	97.14	53.33	59.05	67.62	65.71	88.10	58.57	55.24	69.52	58.57	90.00
Avg.	**90.70**	89.71	71.25	67.80	72.75	65.97	80.00	68.21	63.88	79.78	69.23	85.27

TABLE IV
CLASSIFICATION PERFORMANCE (%) OF SVM CLASSIFIER COMPUTED IN EMOTIONAL MEMORY RETRIEVAL EXPERIMENT (4-CLASS)

Participant	FLM	SLM	FMM mean	FMM mid	LMM mean	LMM mid	FC	RAW mean	RAW mid	RAW all	PCA	ICA
1	**81.43**	76.67	60.48	57.62	41.43	53.81	33.81	22.38	22.38	22.38	21.43	20.95
2	**75.24**	68.57	51.91	41.43	48.09	38.57	48.57	20.95	19.52	31.91	21.90	58.57
3	40.95	**41.43**	34.76	32.38	32.86	32.38	26.19	22.86	22.86	22.86	22.86	22.86
4	**61.90**	57.62	43.33	32.86	40.48	31.43	32.86	21.90	21.90	38.10	21.90	22.38
5	**73.33**	67.62	47.62	31.43	35.24	32.86	22.86	21.90	21.90	21.90	22.38	21.43
6	**85.71**	77.14	49.05	49.52	47.62	47.62	30.95	21.90	23.33	31.43	21.90	22.38
7	**59.05**	57.62	40.95	34.29	32.86	36.67	31.43	30.95	30.00	30.00	30.48	21.90
8	64.29	**64.76**	46.19	28.10	43.33	30.00	27.14	22.38	21.90	22.38	21.90	22.38
9	**51.43**	50.95	35.24	34.29	29.05	24.29	39.05	23.81	24.29	30.95	21.90	22.38
10	**65.71**	54.29	37.62	27.62	36.19	32.86	47.14	26.19	24.76	35.71	22.38	49.52
11	69.05	**70.95**	45.71	44.29	42.38	38.57	61.90	22.38	22.38	24.76	22.38	22.38
12	**54.76**	51.43	40.00	38.10	42.86	45.71	47.14	32.38	37.14	36.67	21.90	20.95
13	**82.38**	78.10	43.33	37.14	50.95	33.33	63.33	21.90	21.43	21.90	20.95	21.43
Avg.	**66.56**	62.86	44.32	37.62	40.26	36.78	39.41	23.99	24.14	28.54	22.64	26.89

classify kitchen utensil, furniture, fear and disgust, where kitchen utensil and furniture belong to the neutral category, and fear and disgust belong to the emotional category (see Table IV).

The results of 2-class and 4-class classification experiments show that we obtain substantially better performances using features extracted for **FLM** and **SLM** compared to the performances of other features. Performance with the ICA and functional connectivity features perform much better than that of the PCA.

We observe that the performances decrease when we use only the middle or mean values of BOLD responses to estimate **FMM-mean**, **LMM-mean**. The performances also decrease for the feature spaces of **RAW-mid**, **RAW-mean** and **RAW-all**. These results show that all of the values of voxel BOLD response carry information to extract a powerful representation for fMRI data.

The emotional memory retrieval experiment data has a drawback for 4-class brain decoding. The number of samples at each run is nearly the same in emotional and neutral categories, which

TABLE V
CLASSIFICATION PERFORMANCE (%) OF SVM CLASSIFIER FOR HCP TASK fMRI DATA

FLM	SLM	FMM mean	LMM mean	FC	RAW mean
96.32	**96.83**	27.28	14.63	90.09	14.28

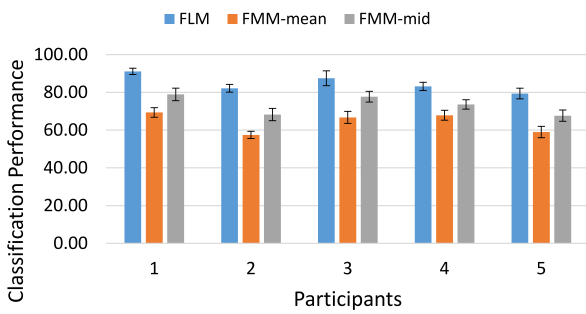

Fig. 5. Mean and standard deviation of classification performances of SVM computed in visual object recognition experiment.

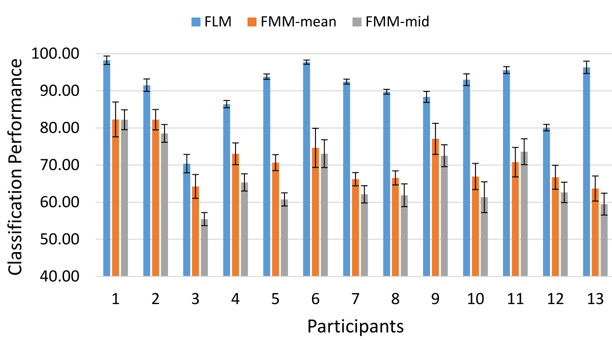

Fig. 6. Mean and standard deviation of classification performances of SVM computed in emotional memory retrieval experiment (2-class).

provides a balanced dataset. However, runs are mostly unbalanced in four subcategories. As a consequence, we observe nearly chance results with raw data when we perform 4-class classification.

Human Connectome Project (HCP) task fMRI Data: Results in Table V reflect that employing **FLM** and **SLM** features are much better to classify cognitive tasks in inter-subject experiments compared to other methods. While, **FMM-mean**, **LMM-mean** and **RAW-mean** give nearly chance results, **FC** also has a discriminative power. This result indicates that a functional connectivity feature, such as Pearson correlation, capture the information content of the data. Considering the long time series of BOLD responses in HCP dataset, this result is expected.

We provide the mean and standard deviations of classification performances obtained by different meshes that are constructed with $p \in \mathcal{P}$ for visual object recognition experiment in Fig. 5, and with $p \in \mathcal{S}$ for emotional memory retrieval experiment in Figs. 6 and 7. In Fig. 5, bars represent the mean classification performance averaged over all $p \in \mathcal{P}$, whereas in Figs. 6 and 7, bars represent the mean classification performance averaged over all $p \in \mathcal{S}$. In these figures, each error bar represents standard deviations of the corresponding performance value. For

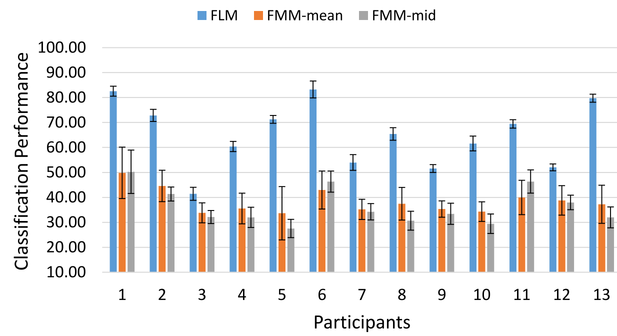

Fig. 7. Mean and standard deviation of classification performances of SVM computed in emotional memory retrieval experiment (4-class).

each participant, the first bar depicts the performance of **FLM** features which is extracted by using the entire temporal measurements of the BOLD responses, whereas the last two bars depict performances obtained using just the mean or middle values of BOLD responses. We observe that standard deviation of performance values obtained using various mesh sizes decreases when temporal measurements are considered for statistical learning of the models. In other words, the methods employing temporal measurements are more robust to changes of mesh size p than the methods which do not employ temporal measurements.

Notice that, the entries of BOLD response vector, $\boldsymbol{x_{w,v}} = [x_{w,v}(t)]_{t=1}^{D}$, at each neighboring voxel, contribute to the estimation of mesh edge weights in the regularized linear model of (1). If a voxel has a noisy entry in the BOLD response vector, the effect of this entry on the estimation of mesh weights, will be relatively small considering the entire time sequence of BOLD response. However, when we take a single value, such as the mean or middle measurement, not only we lose important information about the BOLD response, but also the mesh representation becomes vulnerable to artifacts. Averaging the BOLD response may avoid the effect of noise with the price of too much smoothing, which results in losing the discriminating information of fMRI data among the cognitive states. This fact can be roughly observed when we compare the subject dependent performances of **FLM** and **SLM** to that of **FLM-mean, FLM-mid**, **SLM-mean and FLM-mid** methods. For example, **FLM** performance of first participant in Fig. 6 varies between 96% - 99% whereas **FMM-mean** and **FMM-mid** performances vary between 75% - 91% and 79% - 87%, respectively. The high variance in performances of the mesh representations estimated by single BOLD response value may be attributed to the effect of artifacts hidden in fMRI data.

C. Analysis of Similarity Measures for Neighborhood Selection

Recall that, we have defined functional neighborhood based on the similarity of voxel time series. In this subsection we analyze the effect of different similarity measures on the classification performance. We compare the results of **FLM** formed using Pearson correlation, partial correlation and Granger causality as the similarity measure to select functional nearest neighbors in the visual recognition experiment (see Table VI).

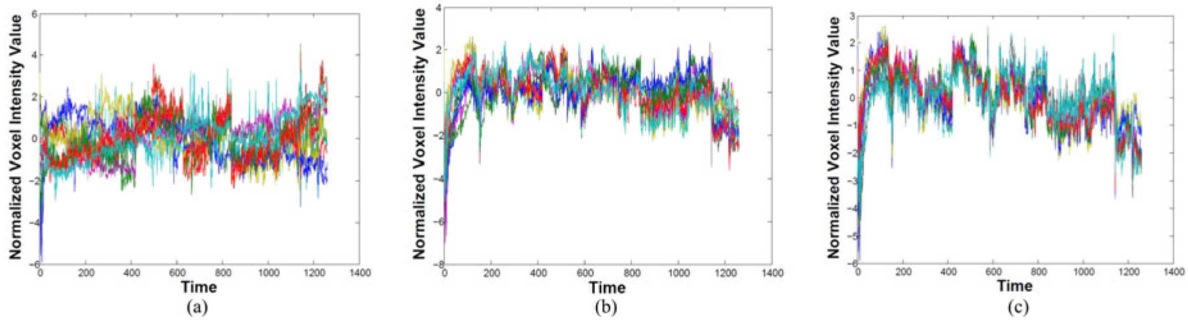

Fig. 8. BOLD responses of a voxel set consisting of 10 voxels. (a) Randomly selected voxels. (b) A random seed voxel with its Spatial Neighbors. (c) A random seed voxel with its Functional Neighbors.

TABLE VI
CLASSIFICATION PERFORMANCE (%) OF SVM CLASSIFIER COMPUTED IN VISUAL OBJECT RECOGNITION EXPERIMENT

P	FLM Corr	FLM Parcorr	FLM Granger
1	91.42	88.33	86.67
2	83.81	87.50	78.24
3	92.86	87.03	87.96
4	89.05	79.63	77.78
5	78.09	81.95	74.07
Avg.	87.04	84.89	80.94

Our results on visual object recognition experiment reflect that selecting functional neighbors based on Pearson correlation leads to better accuracy compared to partial correlation or Granger causality to select the neighbors of seed voxels. We also observe that meshes formed by Granger causality have the lowest classification performance on this dataset.

D. Analysis of Local Meshes

The major assumption of the proposed mesh representation is that the voxel BOLD responses are similar to each other at a predefined locality, so that a BOLD response of a voxel can be represented by a linear combination of the BOLD responses of its nearest neighbors. In other words, we assume that the error of a regularized linear regression model is small enough such that a cognitive stimulus can be represented by a set of local meshes, where the edge weights of the meshes can be estimated by minimizing the expected square error.

1) Statistical Analysis of Correlations of Voxels: In order to understand how voxels within a neighborhood behave, and how their behavior differs from the behavior of random voxel sets, we plot a seed voxel with $i)$ a set of randomly selected voxels (Fig. 8(a)), $ii)$ its ten spatially (Fig. 8(b)) and $iii)$ ten functionally (Fig. 8(c)) nearest neighbors. We observe that, sample voxels located within spatial and functional neighborhoods perform similar under presentation of the same stimuli.

Although we select spatially or functionally closest voxels as neighbors, we need to further analyze the distribution of correlation values between the seed voxels and their neighbors to understand if the closest voxels are also highly correlated. Therefore, we compute pairwise relationship (i.e. correlation) between the seed voxels and the surrounding voxels using Pearson correlation. In our analysis, surrounding voxels are selected as (a) spatially nearest neighbors of seed voxels, and functionally nearest neighbors of seed voxels selected using (b) Granger causality (c) partial correlation (d) Pearson correlation. First, we compute correlations between ten surrounding voxels and the seed voxel. Then, we depict the histograms of all correlations computed for all voxels with their surrounding voxels in meshes.

The normalized Granger causality histogram in Fig. 9(b) reflects that neighboring voxels with maximum Granger causality value may have negative correlations with the seed voxel. On the other hand, the results show that correlation values of the voxels observed with the highest frequency are close to 0.9 when the histograms are computed for meshes formed using spatially (see Fig. 9(a)) and functionally close voxels selected using partial correlation (Fig. 9(c)) and Pearson correlation (Fig. 9(d)). These observations indicate that the voxels modeled in the same mesh have statistical relationship with each other. Therefore, one may expect that the linear relationship among the BOLD responses at a locality, defined by a neighborhood system, provides a reasonable fit to the data.

2) Statistical Analysis of Models: Recall that, we represent the intensity values of each voxel as a regularized linear combination of those values of its p-nearest neighbors in our models. Yet, we obtain a regression error for each mesh for the estimation of seed voxels considering its neighbors. In the next set of experiments, we analyze how well the seed voxels are represented in terms of their nearest neighbors by exploring the model estimation error of the proposed representation.

For this purpose, we employ a goodness of fit measure, called R^2, defined as one minus the residual variation divided by total variation, where residual variation is the summation of square errors obtained from regression model, and total variation is the variance of the distribution of the actual data.

Notice that the R^2 measure takes values between 0 and 1, such that the values closer to one represent better fit of models. In the analysis, we computed R^2 values for all meshes of a participant formed for all samples and around all voxels. In Fig. 10, we plot the histograms for R^2 values computed when the meshes are formed using (a) spatially nearest voxels, and (b) functionally nearest voxels.

In the experiments, if seed voxels of meshes formed using spatial or functional neighbors are represented in terms of their

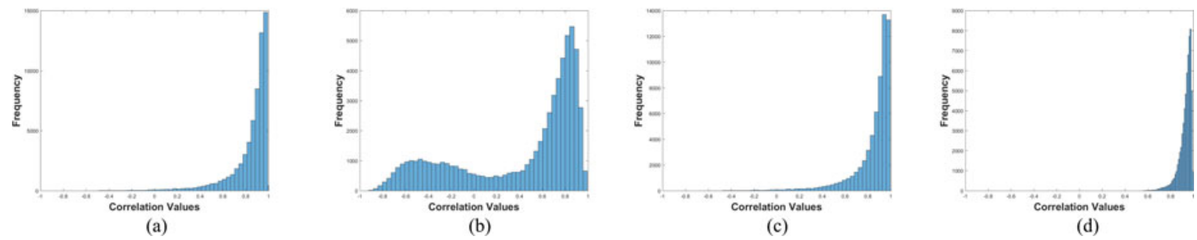

Fig. 9. Histograms of correlations between seed voxels and surrounding voxels. (a) Spatial closeness. (b) Granger causality. (c) Partial correlation. (d) Pearson correlation.

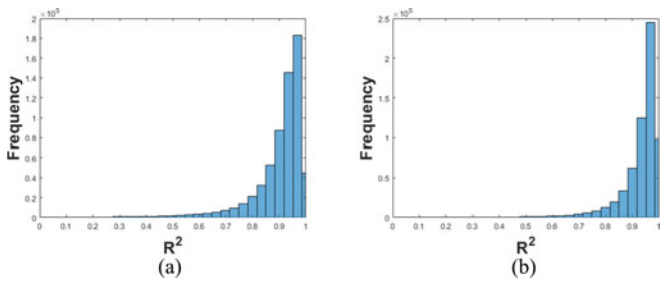

Fig. 10. Histograms of R^2 values. (a) Spatial Neighbors. (b) Functional Neighbors.

neighbors, then we observe that the mean values of histograms for R^2 are 0.90 and 0.93, respectively (Fig. 10(a) and (b)). Therefore, employing spatial or functional neighbors during the construction of meshes results in good model fit, where the latter leads to slightly better fit compared to the former.

VII. Conclusion

In this study, we propose a novel method which maps fMRI measurements, recorded during a cognitive stimulus to a set of local meshes. The proposed method defines two types of local meshes around each voxel, namely spatially local meshes (**SLM**) and functionally local meshes (**FLM**). While **SLM** represents the relationships among voxel BOLD responses in a spatial neighborhood system, **FLM** represents them in a functional neighborhood. Local mesh edge weights enable us to represent the crucial information in fMRI data to characterize the brain states. This fact is verified in brain decoding problems. We observe that **FLM** and **SLM** features perform substantially better compared to the state-of-the-art fMRI features, such as ICA, PCA, Pearson correlation and vectors of raw voxel intensity values, to decode the cognitive states. The decoding performances are first measured in two fMRI datasets, collected by our team while the subjects perform visual object recognition and emotional memory retrieval tasks. Then, comparably high performances are obtained in the publicly available task dataset of Human Connectome Project. The relatively high performances of the local mesh representation partially indicate the validity of the major assumption of this study, that is, the relationship among the voxel BOLD responses can be approximated by a regularized linear model in a predefined locality.

We observe that classification performances of SVM depend on the mesh size p, and varies for each participant. However, the local meshes estimated by the entire time series of BOLD response not only increase the decoding performances, but also decrease the effect of mesh size on performances. This fact is confirmed by measuring the standard deviation of decoding performances as the mesh sizes change. It is observed that when we take the average or the middle values of the BOLD responses, the standard deviation of the performances with respect to the mesh size, increases. Therefore, mesh representations estimated by the entire temporal measurements of BOLD response are robust to the effect of mesh sizes for decoding the cognitive tasks.

A future research direction will be the development of algorithms to generalize the ensemble of local meshes to represent resting state fMRI data for detection of diseases.

Acknowledgment

The authors would like to thank Orhan Firat for designing and recording the visual object recognition dataset, the ImageLab members of METU for insightful discussions and data gathering, and UMRAM Center of Bilkent University for providing the facility and technical support during fMRI recordings.

References

[1] M. Kefayati, H. Sheikhzadeh, H. Rabiee, and A. Soltani-Farani, “Semi-spatiotemporal fMRI brain decoding,” in *Proc. Int. Workshop Pattern Recogn. Neuroimag.*, Philadelphia, PA, USA, Jun. 2013, pp. 182–185.
[2] J. V. Haxby, M. I. Gobbini, M. L. Furey, A. Ishai, J. L. Schouten, and P. Pietrini, “Distributed and overlapping representations of faces and objects in ventral temporal cortex,” *Science*, vol. 293, no. 5539, pp. 2425–2429, 2001.
[3] S. Kloppel, A. Abdulkadir, C. R. Jack, N. Koutsouleris, J. Mourao-Miranda, and P. Vemuri, “Diagnostic neuroimaging across diseases,” *NeuroImage*, vol. 61, no. 2, pp. 457–463, 2012.
[4] G. Orru, W. Pettersson-Yeo, A. F. Marquand, G. Sartori, and A. Mechelli, “Using support vector machine to identify imaging biomarkers of neurological and psychiatric disease: A critical review,” *Neurosci. Biobehav. Rev.*, vol. 36, no. 4, pp. 1140–1152, 2012.
[5] I. Oztekin and D. Badre, “Distributed patterns of brain activity that lead to forgetting,” *Front. Hum. Neurosci.*, vol. 5, no. 86, p. 86, 2011.
[6] F. Pereira, T. Mitchell, and M. Botvinick, “Machine learning classifiers and fMRI: A tutorial overview,” *Neuroimage*, vol. 45, no. 1, pp. S199–S209, 2009.
[7] L. Grosenick, B. Klingenberg, K. Katovich, B. Knutson, and J. E. Taylor, “Interpretable whole-brain prediction analysis with graphnet,” *NeuroImage*, vol. 72, pp. 304–321, 2013.
[8] L. Baldassarre, J. Mourao-Miranda, and M. Pontil, “Structured sparsity models for brain decoding from fMRI data,” in *Proc. IEEE Int. Workshop Pattern Recog. Neuroimag.*, 2012, pp. 5–8.
[9] A. Gramfort, B. Thirion, and G. Varoquaux, “Identifying predictive regions from fMRI with tv-l1 prior,” in *Proc. Proc. IEEE Int. Workshop Pattern Recog. Neuroimag.*, 2013, pp. 17–20.
[10] D. D. Cox and R. L. Savoy, “Functional magnetic resonance imaging (fMRI) brain reading: Detecting and classifying distributed patterns of fMRI activity in human visual cortex,” *NeuroImage*, vol. 19, no. 2, pp. 261–270, 2003.

[11] Y. Kamitani and F. Tong, "Decoding the visual and subjective contents of the human brain," *Nat. Neurosci.*, vol. 8, no. 5, pp. 679–685, 2005.

[12] Y. Kamitani and F. Tong, "Decoding seen and attended motion directions from activity in the human visual cortex," *Curr. Biol.*, vol. 16, no. 11, pp. 1096–1102, 2006.

[13] B. Ng, A. Vahdat, G. Hamarneh, and R. Abugharbieh, "Generalized sparse classifiers for decoding cognitive states in fMRI," in *Proc. Mach. Learn. Med. Imag.*, Beijing, China, 2010, vol. 6357, pp. 108–115.

[14] B. Ng and R. Abugharbieh, "Generalized group sparse classifiers with application in fMRI brain decoding," in *Proc. IEEE Int. Conf. Comput. Vis. Pattern Recognit.*, Colorado Springs, CO, USA, 2011, pp. 1065–1071.

[15] T. M. Mitchell *et al.*, "Learning to decode cognitive states from brain images," *Mach. Learn.*, vol. 57, no. 1–2, pp. 145–175, 2004.

[16] B. Ng and R. Abugharbieh, "Modeling spatiotemporal structure in fMRI brain decoding using generalized sparse classifiers," in *Proc. Int. Workshop Pattern Recogn. Neuroimag.*, Korea, Seoul, 2011, pp. 65–68.

[17] S. P. Pantazatos, A. Talati, P. Pavlidis, and J. Hirsch, "Decoding unattended fearful faces with whole-brain correlations: An approach to identify condition-dependent large-scale functional connectivity," *PLoS Comput. Biol.*, vol. 8, no. 3, p. e1002441, 2012.

[18] J. Richiardi, H. Eryilmaz, S. Schwartz, P. Vuilleumier, and D. V. D. Ville, "Decoding brain states from fMRI connectivity graphs," *NeuroImage*, vol. 56, no. 2, pp. 616–626, 2011.

[19] O. Firat, I. Onal, E. Aksan, B. Velioglu, I. Oztekin, and F. T. Y. Vural, "Large scale functional connectivity for brain decoding," in *Proc. IASTED Int. Conf. Biomed. Eng.*, Zurich, Switzerland, 2014.

[20] C. Baldassano, M. C. Iordan, D. M. Beck, and L. Fei-Fei, "Voxel-level functional connectivity using spatial regularization," *NeuroImage*, vol. 63, no. 3, pp. 1099–1106, 2012.

[21] O. Firat, M. Ozay, I. Onal, I. Oztekin, and F. Y. Vural, "Representation of cognitive processes using the minimum spanning tree of local meshes," in *Proc. Annu. Int. Conf. IEEE Eng. Med. Biol. Soc.*, Osaka, Japan, Jul. 2013, pp. 6780–6783.

[22] J. Richiardi, S. Achard, H. Bunke, and D. V. de Ville, "Machine learning with brain graphs: Predictive modeling approaches for functional imaging in systems neuroscience," *IEEE Signal Process. Mag.*, vol. 30, no. 3, pp. 58–70, 2013.

[23] L. Cossell *et al.*, "Functional organization of excitatory synaptic strength in primary visual cortex," *Nature*, vol. 518, no. 7539, pp. 399–403, 2015.

[24] N. Bazargani and A. Nosratinia, "Joint maximum likelihood estimation of activation and hemodynamic response function for fMRI," *Med. Image Anal.*, vol. 18, no. 5, pp. 711–724, 2014.

[25] N.Kriegeskorte, R. Goebel, and P. Bandettini, "Information-based functional brain mapping," *Proc. Nat. Acad. Sci. USA*, vol. 103, no. 10, pp. 3863–3868, 2006.

[26] M. Ozay, I. Oztekin, U. Oztekin, and F. T. Yarman-Vural, "Mesh learning for classifying cognitive processes," *CoRR*, vol. abs/1205.2382, 2012.

[27] O. Firat, M. Ozay, I. Onal, I. Oztekiny, and F. Vural, "Functional mesh learning for pattern analysis of cognitive processes," in *Proc. IEEE Int. Conf. Cogn. Informat. Cogn. Comput.*, New York City, NY, USA, Jul. 2013, pp. 161–167.

[28] I. Onal, M. Ozay, and F. Yarman Vural, "Modeling voxel connectivity for brain decoding," in *Proc. Int. Workshop Pattern Recogn. Neuroimag.*, Stanford, CA, USA, 2015, pp. 5–8.

[29] E. Mizrak and I. Oztekin, "Relationship between emotion and forgetting," *Emotion*, vol. 16, no. 1, pp. 33–42, Feb. 2016.

[30] D. M. Barch *et al.*, "Function in the human connectome: Task-fMRI and individual differences in behavior," *NeuroImage*, vol. 80, pp. 169–189, 2013.

[31] N. Tzourio-Mazoyer *et al.*, "Automated anatomical labeling of activations in SPM using a macroscopic anatomical parcellation of the MNI MRI single-subject brain," *NeuroImage*, vol. 15, pp. 273–289, 2002.

[32] M. Brett, J.-L. Anton, R. Valabregue, and J.-B. Poline, "Region of interest analysis using an SPM toolbox," in *Proc. 8th Int. Conf. Functional Mapping Human Brain*, Sendai, Japan, 2002.

[33] A. Hyvarinen, "Fast and robust fixed-point algorithms for independent component analysis," *IEEE Trans. Neural Netw.*, vol. 10, no. 3, pp. 626–634, May 1999.

[34] G. Varoquaux, P. R. Raamana, D. A. Engemann, A. Hoyos-Idrobo, Y. Schwartz, and B. Thirion, "Assessing and tuning brain decoders: Cross-validation, caveats, and guidelines," *NeuroImage*, vol. 145, pp. 166–179, 2016.

Itir Onal (S'13) received the B.Sc. and M.Sc. degrees in computer engineering from Middle East Technical University, Ankara, Turkey, in 2011 and 2013, respectively. She is currently working toward the Ph.D. degree in computer engineering at Middle East Technical University, Ankara, Turkey. Between July 2016 and September 2016, she was a visiting research scholar in Delft University of Technology, Delft, Netherlands. Her research interests include biomedical signal processing, computational neuroscience, and pattern recognition.

Mete Ozay (M'09) received the Ph.D. degree in computer engineering from Middle East Technical University, Ankara, Turkey, in 2013. He is currently an Assistant Professor at the Graduate School of Information Sciences, Tohoku University, Sendai, Japan. His current research interests include pure and applied mathematics, information theory, and theoretical computer science.

Eda Mizrak received the B.A. degree in psychology and B.A. degree in business administration from Istanbul Bilgi University, Istanbul, Turkey in 2009 and the M.Sc. degree in clinical psychology from University of Wales, Cardiff, U.K., in 2011 and the Ph.D. degree in psychology from Koc University, Istanbul, Turkey in 2017. Between February 2016 and January 2017, she was a visiting research scholar in the University of California, Davis, CA, USA. She is currently working as a Postdoctoral Fellow in the Center for Neuroscience, University of California, Davis. Her research interests are forgetting of emotional material, working memory, cognitive control, and computational modeling.

Ilke Oztekin received the Ph.D. degree from New York University, New York, NY, USA, in 2008. She worked as a Postdoctoral Research Associate at the Department of Cognitive and Linguistic Sciences, Brown University. She is currently an Associate Professor at the Department of Psychology, Ko University, where she joined in Fall 2010. Her primary areas of expertise are experimental psychology and cognitive neuroscience, with specific emphasis on human memory and cognitive control. Her research has been funded by the European Commission and the Scientific and Technological Council of Turkey (TUBITAK). She received the American Psychological Association Dissertation Research Award (2006), American Psychological Association Division 3 New Investigator Award in Experimental Psychology (2011), Science Academy Young Investigator Award (2013), TUBITAK Encouragement Award (2016), and Turkish Academy of Sciences Outstanding Young Scientist Award (2016).

Fatos T. Yarman Vural (SM'98) received the B.Sc. degree from the Technical University of Istanbul, Istanbul, Turkey, the M.Sc. degree from Bogazici University, Istanbul, and the Ph.D. degree from Princeton University, Princeton, NJ, USA in 1973, 1975 and 1981, respectively. She worked as an Assistant Professor at Drexel University and was a Research fellow at Massachusetts Institute of Technology, Cambridge, MA, USA between 1985 and 1987. She is currently a Professor in the Department of Computer Engineering, Middle East Technical University, Ankara, Turkey. Her research areas include machine learning, pattern recognition, computer vision, and image processing.